Determination of Pressure Drop in Positive Dilute Phase Pneumatic Teff Grain Conveyor Using Experimental CFD-DPM Simulation and ANN Modeling Approach

Lemi Demissie Boset[1,*], Zewdu Abdi Debele[2] and Amana Wako Koroso[1]

[1]*School of Mechanical, Chemical and Material Engineering, Adama Science and Technology University, Adama, Oromia, 0000, Ethiopia*
[2]*Faculty of Agriculture, University of Eswatini, Luyengo, Eswatini, M205, Eswatini*
E-mail: lemi.demissie@astu.edu.et
[*]*Corresponding Author*

Received 29 November 2024; Accepted 17 July 2025

Abstract

Pressure drop in pneumatic conveying systems significantly influences both system performance and energy efficiency. This study combines laboratory experiments with computational fluid dynamics (CFD) simulations to create a predictive model for the pressure drop coefficient using artificial neural networks (ANN), focusing on key components such as feeders, horizontal and vertical pipes, bends, and cyclone separators. Laboratory experiments yield crucial empirical data that validate the CFD simulations, which provide in-depth analyses. The findings reveal a strong correlation between the calculated pressure drop coefficient (K) and the square of the inlet air velocity, expressed as K α v^2. The regression coefficients (R^2) for various components are as follows: feeder ($R^2 = 0.982$), horizontal pipe ($R^2 = 0.989$), vertical

International Journal of Fluid Power, Vol. 26_3, 343–380.
doi: 10.13052/ijfp1439-9776.2631

pipe ($R^2 = 0.991$), bends ($R^2 = 0.972$), and cyclone separator ($R^2 = 0.942$). These results indicate that the model can lead to more efficient designs that accurately reflect real-world conditions, thereby enhancing the overall performance of pneumatic grain conveying systems.

Keywords: Pressure drop, pneumatic conveyor, CFD-DPM simulation, ANN model, pressure drop coefficient, Teff grain.

1 Introduction

Teff is a smallest grain in the world, making it challenging to handle without loss. It is a gluten-free grain that offers significant nutritional benefits and has caught the attention of the modern food industry. However, due to its status as a newer raw material, there is limited information on how to handle and process effectively. In Ethiopia, traditional practices dominate the production and processing of Teff. There is a lack of optimal techniques for sowing, threshing, cleaning, separating, handling, and transporting this grain [1]. It is estimated that 25–30% of teff may be lost before and after harvest, with lodging potentially causing yield losses of up to 30% [2]. Teff seeds are typically broadcast by hand at a rate of 25–50 kg per hectare, but studies suggest that reducing the seed rate to 2.5 to 3 kg per hectare is more efficient. Post-harvest losses in the rural-urban value chain typically range from 2.2 to 3.3 percent, varying with storage conditions and transportation methods used. The handling of teff grain is influenced by its flow ability, measured by the angle of repose, which ranges from 24.09° to 26.16° for different Teff varieties. All teff varieties fall into a very free-flowing category, allowing for transport using gravity or minimal energy [3]. Two main factors complicate the mechanization of Teff. First, it's extraordinarily small grain size, at about 1/150th the size of a wheat grain, affects planting, threshing, and handling. Second, the tendency of teff grass to lodge makes harvesting and threshing more difficult. While much research has focused on its agronomy, grain-related studies are often approached from an engineering perspective. Collaborative research is essential to improve Teff grain quality, boost production, and enhance handling processes [2–4]. Some studies suggest using the aerodynamic characteristics of materials used to design pneumatic conveying and separation systems for Teff grain.

These characteristics are calculated based on the terminal velocity of single particles, but they fail to account for how particle concentration in the air stream affects bulk material behavior in pneumatic systems [5]. Most

researchers recognize that challenges associated with handling Teff due to its tiny size, yet there is a notable lack of studies focused on finding effective solutions to these difficulties. While numerous research papers examine the engineering properties of Teff grain, none have successfully identified methods to minimize losses while preserving quality during handling. Consequently, investigating the pneumatic conveying characteristics of Teff grain is essential for gathering critical data that lead to the development of an efficient pneumatic system that reduces manual labor and costs, minimizes grain loss, and ensures quality and sanitary Teff grain handling process.

Pneumatic conveying is a widely used method for transporting bulk materials in various industries, including food, agricultural pharmaceuticals, and chemicals industries [6]. because it offers many benefits over conventional mechanical conveyor systems, in recent years pneumatic conveyors have gained popularity as a grain handling solution because of their great adaptability, versatile handling application, used for different variety of grains, including moving grains over large distances, along curves, and even vertically. Improve efficiency and smooth integration is also possible since they are simple to incorporate into grain handling systems. Furthermore, the seamless integration and increased efficiency of pneumatic conveyors can be achieved with ease grain handling systems. According to this information, it has great advantage over mechanical conveyor to use a pneumatic conveying system for Teff grain, not only for transporting but also for panting cleaning and treatment. The study related to pneumatic Teff grain conveyors is crucial for the design and optimized pneumatic conveying system for Teff grain.

[7] The work on Predicting Horizontal Pneumatic Conveying of Large Coal Particles Using a Discrete Phase Model focuses on large particles ($>$5 mm), as there are few studies on such sizes. To forecast the horizontal pneumatic conveyance of big coal particles, coupling methods based on the Euler-Lagrange approach and discrete phase model (DPM) were utilized in the simulated study.

Pressure drop in pneumatic conveying systems is influenced by various factors, such as the properties of the conveyed material, the geometry of the conveying system, and the operating conditions. One of the most challenging components in pneumatic conveying systems is the 90° bend, which can significantly contribute to the overall pressure drop [8].

The pressure drop in a 90° bend is influenced by factors such as the bend radius, the cross-sectional area of the bend, and the velocity of the conveyed material. Performance of pneumatic conveyance systems, which are extensively used in many industries to move large goods, poses a special challenge

to comprehension and improvement. In order to tackle this difficulty, sophisticated particle-tracking models combined with computational fluid dynamics (CFD) simulations have become effective instruments for examining the intricate relationships between solid particles and fluid flow [9] common numerical techniques used in pneumatic conveyor studies are CFD-DEM and CFD-DPM [10].

ANSYS Fluent was used to create a 3D computational fluid dynamics (CFD) model that simulated the two-phase flow across the 90° bends. The air and teff grain phases were modeled using the Euler-Lagrange method [11]. To capture the turbulent effects, the realizable k-ε turbulence model was used. For pressure and velocity coupling, the SIMPLE solution approach with a pressure-based solver was employed. The discretization of momentum, turbulence kinetic energy, and turbulence dissipation rate equations were done using second-order upwind schemes [12]. The pressure drop across the bend was computed using the CFD results from the surface integral result for area weighted average static pressure for the created plane that is perpendicular to the bend pipe's axis [13].

[14] Cyclone separators are commonly used in pneumatic conveying systems due to their simplicity, efficiency, and low cost. In this process, a mixture of gas and solid particles is conveyed through a pipeline, and the particles are separated from the gas stream using a cyclone separator [15] cyclone separators are designed to separate grains from gas or to transport milled material, and their specific application and design may vary depending on the context and the materials being processed. The Lapple model is one of the most widely used models for predicting the performance of cyclone separators it is based on the principle of inertial impaction, where the particles are separated from the gas stream based on their size and inlet air velocity. Because of its simplicity, [16] the Lapple model to be effective in predicting the performance of cyclone separators in various applications.

The literature review has identified a potential research gap in the experimental and CFD-DPM investigations of pressure drop for a pneumatic Teff grain conveyor system. The experimental approach involves conducting experiments in a laboratory setting to measure the pressure of the pneumatic conveying system under different operating conditions. The experimental data is then used to validate the numerical model. Validating the accuracy and reliability of a model through the comparison of simulation results and experimental data is essential, particularly for predicting the pressure drop in pneumatic conveying system. By utilizing experimental data and numerical simulations, this study aims to analyze the pressure drop in a pneumatic

Teff grain conveying system. The findings are expected to significantly enhance the design and optimization of these systems, resulting in improved efficiency, cost savings, and better product quality [17].

Using an artificial neural network (ANN) model for pneumatic conveyor systems presents numerous advantages compared to traditional regression models, especially when it comes to managing the inherent complexities and nonlinearities that characterize these systems. Unlike conventional regression approaches, which often rely on linear assumptions and may struggle to accurately capture the intricate relationships between variables, ANNs are designed to learn from data in a more flexible and adaptive manner [18]. This capability allows them to effectively model the dynamic behavior of pneumatic conveyors, where factors such as airflow, material properties, and system configurations can interact in complex ways. Furthermore, ANNs can process large datasets and identify patterns that might be overlooked by simpler models, leading to improved predictions and optimizations in system performance. By leveraging the power of machine learning, ANN models can enhance the efficiency and reliability of pneumatic conveyor systems, making them a superior choice for engineers and operators seeking to improve operational outcomes [19, 20].

Various research findings indicate that ANN are among the most effective methods for modeling pressure drops in pneumatic conveyors, crucial for transporting bulk materials. Accurately predicting pressure drop optimizes performance and energy efficiency, yet traditional methods struggle with the complex interactions and nonlinearities of pneumatic systems. ANNs excel by learning from large datasets, capturing intricate patterns that reflect system behavior under varied conditions. By training on historical data, ANNs yield precise pressure drop predictions, enabling engineers to design more efficient conveying systems. As research in this area progresses, the application of ANN not only deepens the understanding of pneumatic dynamics but also drives advancements in automation and process optimization, solidifying its role as a leading modeling approach.

2 Materials and Methods

Eight new varieties of Teff were collected according to the year of released such as Boset, Kora, Dagim, Felagot, Bora Ebba, Bishoftu, and Boni were obtained from Debre Zeit Agricultural Research Center of the Institute of Agricultural Research in Ethiopia (EIAR). The Ethiopian Institute of Agricultural Research (EIAR)'s National Teff Improvement Program

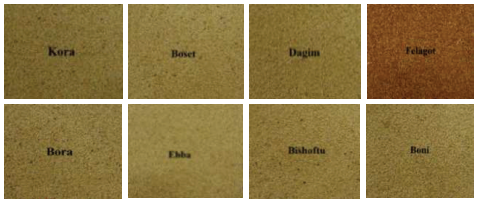

Figure 1 Different varieties of Teff grain

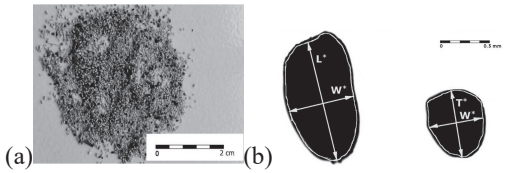

Figure 2 (a) Image of Teff grain (b) gimension of grain.

distributed such Teff species. The laboratory tests were conducted at Adama Science and Technology University, Chemical Department Laboratory.

An oven method can be used directly to determine the moisture content of eight different types of teff grain.

$$MC = \frac{(w-d)}{w} \times 100 \tag{1}$$

Moisture content of eight different types of Teff grain measured according to ASAE standards S3523 (ASAE, 1994). Recorded moisture content for each variety of Teff grain is 9.14%–15%, 7.73%–13.48%, 10.14%–14.35%, 9.5%–15.28%, 11.59%–14.14%, 9.5%–13.36%, 10.25%–12.36%, and 8.65%–11.96% for Felagot, Ebba, Bishoftu, Dagim, Boni, Boset, Kora, and Bora, respectively. Particle size distribution of dimensions 20 pieces of Teff seeds were used where dimensions of each seeds: length L (mm), width W (mm), thickness T (mm), were determined by digital image analysis using ImageJ software from pictures which were taken with the aid of a trio ocular microscope [21]. Geometric mean diameter $D_g = 0.68$ mm and arithmetic mean diameter $D_a = 0.72$ mm.

Geometric mean diameter D_g(mm) and Arithmetic mean diameter D_a(mm) calculated using the following equation

$$D_g = \sqrt[3]{W \times T \times L} \tag{2}$$

$$D_a = \frac{W+T+L}{3} \tag{3}$$

Table 1 Summary of measured teff grain size

Teff Variety	Width (mm)	Thickness (mm)	Length (mm)	Projected Area (mm^2)	Thousand Grain Weight (g)
Boset	0.63±0.05	0.56+0.10	1.01±0.13	0.50±0.07	292.44±42.93
Kora	0.68±0.10	0.57+0.06	1.09±0.18	0.58±0.12	297.46±462
Dagim	0.67±0.08	0.61+0.07	1.17±0.17	0.61±0.09	304.01±41.58
Felagot	0.52±0.07	0.52+0.08	0.92±0.08	0.42±0.06	251.82±14.38
Bora	0.58±0.09	0.56+0.04	1.10±0.18	0.50±0.11	276.57±38.15
Ebba	0.70±0.08	0.58+0.12	1.09±0.15	0.60±0.10	287.65±43.39
Bishoftu	0.59±0.14	0.54+0.08	0.94±0.15	0.44±0.12	279.39±36.47
Boni	0.59±0.09	0.53+0.03	0.94±0.15	0.44±0.12	287.42±43.63

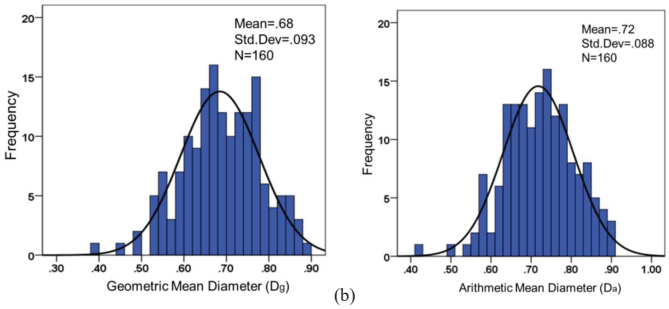

(a) (b)

Figure 3 (a) Geometric mean diameter (b) arithmetic mean diameter.

The study consider practical application in local for feeding Teff milling machine, small scale Teff grain milling machine its capacity is 300 kg/h–500 kg/h which is mostly used in local milling house, therefore (ms) for desired dilute phase pneumatic conveying system is 360 kg/h or 0.1 kg/s. The study used blower with air flow rate 19 m^3/min. A solid loading ratio, or phase density, is a useful parameter in helping to visualize the flow. It is ms/ma. Maximum recommended solid loading ratio for dilute phase pneumatic conveyor is 15. Solid loading ratio (μ) is

$$\mu = \frac{m_s}{m_a} \tag{4}$$

Use the method of Rizk to predict the gas velocity at saltation using calculated solids loading ratio mass flow rate for Teff grain.

$$\mu = \frac{1}{10^{\delta}} \left(\frac{U_o}{(gD)^{1/2}} \right)^{\chi}$$

$$\chi = 1.1d_p + 2.5 \quad \text{and} \quad \delta = 1.44d_p + 1.96 \tag{5}$$

Table 2 Minimum conveying velocity

Blower Air Flow Rate		Pipe Area(m^2)		Air Velocity(m/s)	
		D1 = 46 mm	D2 = 71 mm	D1 = 46 mm	D2 = 71 mm
Q(m^3/min)	Q(m^3/s)	A2(m^2)	A1(m^2)	u_2(m/s)	u_1(m/s)
2	0.033	0.0016	0.0039	20.07	8.42
4	0.067	0.0016	0.0039	40.14	16.85
6	0.100	0.0016	0.0039	60.20	25.27
8	0.133	0.0016	0.0039	80.27	33.69
10($\eta = 52.6\%$)	0.167	0.00166	0.0039	100.34	42.12

The value of χ and δ is equal to 3.215 and 2.896 respectively; design air velocity is must be greater than saltation velocity, the design velocity is superficial gas velocity (v) is calculated from saltation velocity as:

$$v = 1.5U_o \tag{6}$$

The solid loading ratio (μ) is 2.22, with corresponding salt velocities (U_o) of 6.85 m/s for a pipe diameter of 46 mm and 8.51 m/s for a pipe diameter of 71 mm. Additionally, superficial gas velocity (v) are measured at 10.27 m/s for the 46 mm diameter and 12.76 m/s for the 71 mm diameter.

2.1 Design of Pneumatic Teff Grain Conveyor System

Designing a pneumatic teff grain conveyor system layout involves several considerations to ensure efficient and effective teff grain handling. Certain standards in dilute phase pneumatic conveying, the solid loading ratio typically ranges from (2% to 15%), Laboratory experiment for dilute phase pneumatic conveyor has some standards pressure must be measured between (2–3 m) gap to get a significant pressure drop. The ratio of bend radius to pipe bore diameter must be greater than (6) to minimize pressure drop in the system. There are three kinds bends in any pneumatic conveyor bends connect horizontal pipeline to horizontal pipeline (H-H), bends connect horizontal pipeline to vertical pipeline (H-V) and bends connect vertical pipeline to horizontal pipeline (V-H) because of the system must be include Horizontal, Vertical and Bends and there different configurations. Design of pneumatic conveyor is focus on horizontal pipeline, pressure drop in horizontal pipeline is slightly high than vertical pipeline, in pneumatic conveyor most of pipeline is composed from horizontal pipeline. Minimum horizontal pipeline length is 20 feet or 6 m in laboratory test of pneumatic conveyor. It is important to consider that the minimum conveying air velocity for dilute phase conveying

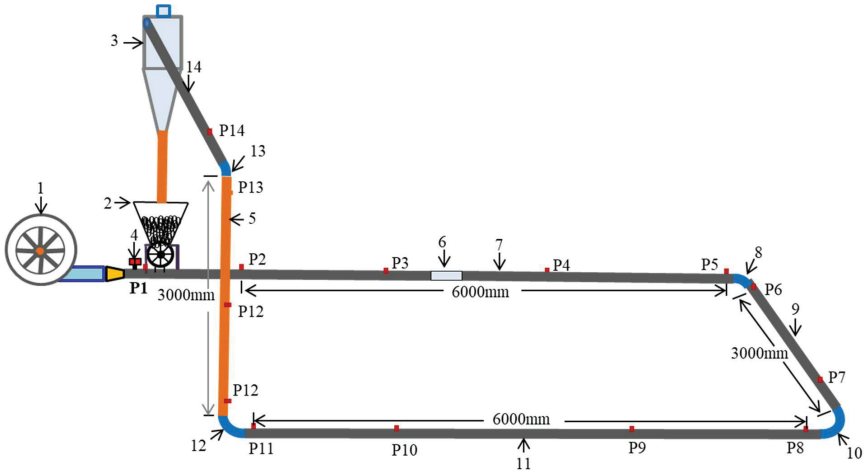

Figure 4 Experimental set up for measurement of pressure drop due to feeder 1: blower; 2: rotary feeder; 3: cyclone separator; 4: air flow control valve; 5: vertical pipe; 6: sight pipe; 7, 9, 11, 14: horizontal pipe; 8, 10, 12, 13: bends; 10: P1-P14: pressure transducer.

is about 11 m/s and additionally, for dilute phase conveying systems, the minimum velocity is typically of the order of 15 m/s, and if it drops by more than about 10% or 20%, the pipeline is considered to be blocked. Design of Pneumatic Teff Grain Conveyor System Layout Standard pipeline configuration in a pneumatic Teff grain conveyor system typically consists of horizontal piping, vertical piping, and bends. The pressure rating of the conveying pipeline should be suitable for the maximum conveying pressure of the system, and the pipeline should be designed to prevent blockages and build-up. The design should ensure that the solids velocity in the pipeline does fall below the minimum required to maintain efficient Teff grain flow.

The feeding mechanism is Rotary Feeder because of particular advantages of using rotary feeders for positive pressure conveying lines are that minimum headroom is required, there are no moving parts and, if the device is correctly designed, there need be no air leakage from the feeder, as there is with nearly all other types of feeder. A rotary basically consists of a controlled reduction in pipeline cross section in the region where the material is fed from the supply hopper, as shown in Figure:

To calculate the bulk Teff grain flow rate from a hopper, the flow rate of bulk Teff grain from a hopper depends on various factors such as the hopper discharge rate, outlet diameter, Teff grain bulk density, internal friction, wall friction, and the inclination of the hopper. Here is method and equations that

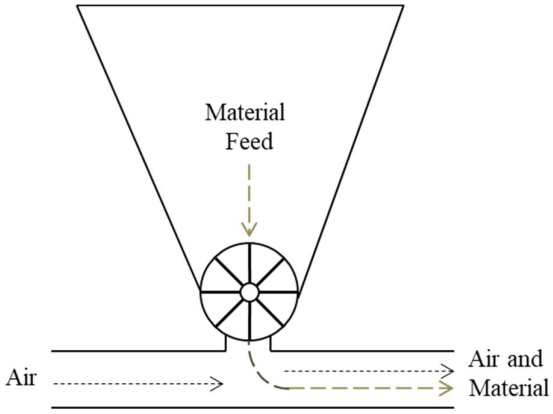

Figure 5 Rotary feeder.

can be used to calculate the Teff grain material flow rate from a hopper for pneumatic conveyor feeder.

$$\dot{m}_s = \frac{B^2 \rho_b \sin(\theta)}{2[1 - \sin(\theta)]} \tag{7}$$

Where: $\dot{m}_s$ = hopper discharge rate in kg/s B = outlet diameter of the hopper in m ρ_{b} = powder bulk density g = gravitational acceleration and θ = hopper half-angle. According to many research studies, Teff grain has a lower angle of repose than other grain. As a result, it falls within the category of very free flow material.

2.2 Calculation of Pressure Drop in Pneumatic Conveyor

In a dilute phase pneumatic conveyor system for Teff grain, several key variables must be taken into account, including the physical properties of the Teff grain, the characteristics of the air used in the system, and the dimensions of the pipe. The properties of Air, Teff grain characteristics, and pipe size are summarized in Table 3. Notably, the calculations for air properties include the universal gas constant, which is R = 287 J/kg·K, and the standard air density, which is $\rho_{\mathrm{a}} = 1.22$ kg/m^3.

After determine the properties of Teff grain, air characteristics, and pipe size total pressure calculated as follows:

$$\Delta P_{total} = \Delta P_{accel} + \Delta P_{lift} + \Delta P_{bends} + \Delta P_{air} + \Delta P_{solids} \tag{8}$$

Table 3 Air property, material characteristics and pipe size

Material	Teff Grain
Desired mass flow rate	300–500 kg/hr
Mean Particle density	1120 kg/m^3
Mean Particle size Diameter	0.68 mm
Pipe diameter	46 mm, 71 mm and 102 mm
Horizontal length	18 m
Vertical lift	3 m
Number of bends	4
Bend constant	0.5
Solid loading	2.08–4.17
Air density	1.22 kg/m^3

The design superficial gas velocity (v) is calculated from saltation velocity

$$v = 1.5U_o \tag{9}$$

The solid velocity (us) is calculated from saltation velocity from table 1.6, where $d_p = 0.00068$ m, and $\rho_s = 1120$ kg/m^3.

$$u_s = U_o(1 - 0.0638d_p^{0.3}\rho_s^{0.5}) \tag{10}$$

The porosity (ε) was calculated from solid flux (G_s) and solid flux is Ratio of solid mass flow rate (m_s) to area (A). The porosity always 0.99 for dilute phase pneumatic conveyor. The interstitial gas velocity (u_g) is from Saltation velocity (U_o) and porosity (ε)

$$u_g = \frac{U_o}{\varepsilon} \tag{11}$$

The slip velocity (u_{slip}) is calculated from interstitial gas velocity.

$$u_{slip} = u_g - u_s \tag{12}$$

In this particular case, we use the conventional friction factor formulation we learned in fluid mechanics. If the conveying line is operated as "air only", then this number is relatively easy to either check with a gauge or hand held manometer near the blower. Note that the gas density needs to be evaluated at each point in the pipe consequently, design calculations usually are done by breaking the line into many small pieces by using Darcy–Weisbach equation.

2.2.1 Pressure due air friction

$$\Delta P_{air} = \frac{\lambda_f \rho_g L v^2}{2D} \tag{13}$$

Turbulent flow (i.e., Re $>$ 2300): Using dimensional analysis, as in laminar flow case can be obtained. λ_{f} is calculated by the following equations, Reynolds number (Re) is

$$Re = \frac{\rho_a v D}{\mu_d} \tag{14}$$

Where $\rho =$ Air density, v $=$ Air velocity, D $=$ Pipe bore diameter (m) and $\mu_{\mathrm{d}} =$ Dynamic viscosity of air and the value of $\rho_{\mathrm{a}} = 1.22$ kg/m^3 and $\mu_{\mathrm{d}} = 0.0000184$ kg/m.s. Reynolds number:

Gas friction factor (λ_{f}) is

$$\lambda_f = \frac{1.325}{\left(\ln\left[\frac{K_s}{3.7D} + \frac{5.74}{\mathrm{Re}^{0.9}}\right]\right)^2} \tag{15}$$

For Common Pipes

$$\frac{K_s}{D} \approx 0.001$$

2.2.2 Pressure drop due to particle acceleration

The particles are required to accelerate after being introduced into the line – note that this is a onetime effect in the calculation here v and up are the particle and gas velocities respectively.

$$\Delta P_{acc} = \mu v \rho_g u_s \tag{16}$$

2.2.3 Pressure drop due to lift

Standard treatment here as we would expect ε is the voidage and for dilute phase systems willtend to be 0.99 or greater and $\rho_{\mathrm{p}} = 1120$ kg/m^3, $\varepsilon = 0.99$, Δz $= 3$ m, g $= 9.81$ m/s^2 and $\rho_{\mathrm{g}} = 1.22$ kg/m^3. For vertical pipeline, Modified Hinkle Correlation:

$$\Delta P_{lift} = \rho_p (1 - \varepsilon) \Delta z g + \varepsilon \rho_g \Delta z g \tag{17}$$

2.2.4 Pressure drop due to bends

Bends are quite common in conveying systems and numerous correlations have been developed to calculate bend pressure drop pressure drop in the field, it needs Note that when measuring to be measured several pipe

diameters downstream of the exit of the elbow to properly account for particle reacceleration after the bend.

$$\Delta P_{bend} = \frac{B(1+\mu)\rho_g v^2}{2D} \tag{18}$$

Where $R_B =$ bend radius

R_B/D	2	4	≥6
B	1.5	0.75	0.5

2.2.5 Pressure drop due to solids friction

The solids friction component mirrors that of gas pressure loss except for now us has a special "solids friction factor". There are some existing correlations for λ_Z both in the vertical and horizontal direction. The friction factor can also be determined from either pilot plant work or by careful analysis of a production plant.

$$\Delta P_{solids} = \frac{\mu\lambda_Z\rho_g L v^2}{2D} \tag{19}$$

Solid friction factor (λ_z) according to Weber proposed in 1982:

$$\lambda_z = K\mu^a Fr^b Fr_s^c \left(\frac{D}{d_p}\right)^d \tag{20}$$

Where Fr = Froude number for gas and Frs = Froude number for solid

	K	a	B	C	d
Fine powder	2.1	−0.3	−1	0.25	0.1
Coarse powder	0.082	−0.3	−0.86	0.25	0.1

$$Fr = \frac{u_g}{\sqrt{gD}} \tag{21}$$

Particle terminal is important velocity parameter of a two-phase flow, which depends on the drag coefficient thus, on the Reynolds number as well.

$$u_t = 1.74\left[\frac{d_p\left(\rho_s - \rho_a\right)g}{\rho_a}\right]^{0.5} \tag{22}$$

For $500 < \mathrm{ReT} < 2 \times 10^5$

$$Fr_s = \frac{u_t}{\sqrt{gd_p}} \tag{23}$$

$$\lambda_z = K\mu^a Fr^b Fr_s^c \left(\frac{D}{d_p}\right)^d \tag{24}$$

2.2.6 Pressure drop due to feeder

To develop a model for the pressure drop coefficient (K) in a pneumatic conveyor when all variables are measured from laboratory tests, we can use regression analysis to determine the relationship between K and the other variables. Here's a suggested approach: The pressure drop across feeder essentially depends on the material flow rate and air flow rate [22, 23]. Generally pressure drop coefficient is often defined as:

$$\Delta P = \frac{1}{2} K \rho_g v_i^2 \tag{25}$$

Where, ΔP pressure drop, ρ_g is gas density, v_i is inlet velocity, and K is pressure drop coefficient

2.2.7 Pressure drop due to cyclone separator

The pressure drop across a cyclone essentially depends on the cyclone dimensions and operating conditions [24]. Generally; it is proportional to the gas inlet velocity head and is often defined as:

$$\Delta P = \frac{1}{2} \rho_g v_i^2 N_H \tag{26}$$

Where, ΔP is cyclone pressure drop, ρ_g is gas density, v_i is inlet velocity, and N_H is a number of velocity heads, and it is a pressure drop parameter to account for all pressure drop components in terms of inlet velocity heads.

$$N_H = 16 \frac{WH}{D_e^2} \tag{27}$$

Where it is a dimensionless metric that measures the pressure drop across the cyclone, the number of velocity heads (NH) is also known as the pressure drop coefficient for a cyclone separator.

Gas-solid interactions, pressure drops, and flow characteristics are only a few of the complex dynamics involved in pneumatic conveying systems. For industrial applications, research focuses mostly on scaling up to make sure that systems operate well at higher scales. Many researches prioritize scaling because of this intricacy, requiring for a thorough understanding of how different characteristics vary with scale [25, 26].

Cyclones separator for different application are usually based on the standard dimension.

Lapple Model was developed based on force balance without considering the flow resistance. Lapple assumed that a particle entering the cyclone is

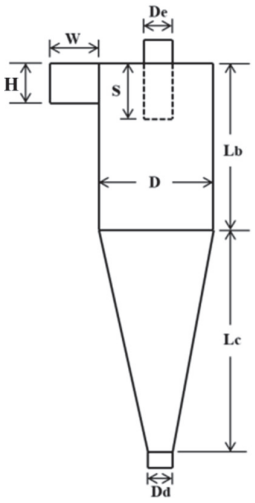

Figure 6 Cyclone dimension Lapple model.

Table 4 Lapple model cyclone separator dimensions

Lapple Model Cyclone Separator Dimensions (mm)	Dimensions	Ratio
Diameter od cyclone Body (Barrel)	D	4W
Length of the Body	L_b	2D
Length of the Cone	L_c	2D
Height of the Inlet	H	D/2
Diameter of Gas Exit	D_e	D/2
Diameter of Dust outlet	D_d	D/4
Length of vortex Finder	S	5D/8
Total length of cyclone	$L_b + L_c$	4D

evenly distributed across the inlet opening. The particle that travels from inlet half width to the wall in the cyclone is collected with 50% efficiency [27]. A study cyclones with different inlet shapes and found that under the same inlet area, conducted CFD simulations the separation performance of cyclones with circular inlets was similar to those with rectangular or elliptical inlets. The area of inlet duct of cyclone separator was similar with bore area pneumatic conveyor pipeline. Cyclone separator Inlet Dimension: [17] Standard Cyclone Dimension Lapple Dimension conventional Dimension is used to determine over all dimension of cyclone and all calculated cyclone dimension is as shown in table below.

The inlet air velocity is depend on blower capacity, pipe diameter and solid loading ration as design of dilute phase pneumatic conveyor for teff

grain. In design of dilute phase pneumatic conveyor of teff grain is minimum air velocity or superficial air velocity is calculated from saltation of teff grain in horizontal pipeline. Air ratio is from 9.55 m/s–15 m/s and solid loading ratio is 2–4.

In this study, we investigate the pressure drop in a pneumatic conveying system specifically designed for Teff grain, utilizing a combination of experimental measurements and CFD-DPM simulations. The experimental setup is designed to employ a digital anemometer to accurately measure the inlet air velocity, while a digital manometer is utilized to record the pressure drop across the cyclone separator. To effectively capture the complex flow dynamics within the cyclone, the k-epsilon RNG swirling-dominated turbulence model is employed in the simulations, which is a well-suited turbulent model for handling complex flow characteristics throughout the cyclone separator. This comprehensive approach aims to enhance our understanding of the pressure drop behavior in cyclone separators and provide valuable information for the optimization of the pneumatic Teff grain conveying system.

2.3 CFD-DPM Model

In CFD-DPM simulation, number iteration depends up on scaled residuals. When scaled residuals approach to zero and less than (1E-5)-(1E-6) the simulation became converged. The equations used to compute the trajectory of the discrete phase particle is given as follows:

$$\frac{du_p}{d_t} = Fd(u - u_p) + \frac{g(\rho_p - \rho)}{\rho_p} + F \tag{28}$$

Where u_p and u are the particle and fluid velocities, respectively, ρ_p and ρ are the particle and fluid densities, respectively. The drag force, Fd, acting on a spherical particle is

$$F_d = \frac{18\mu C_D Re}{\rho_p d_p^2 24} \tag{29}$$

Where Re is the Reynolds number, μ is the dynamic viscosity of the fluid, and CD is the drag coefficient based on the shape of the particle [28].

2.4 Turbulence Model

Reynolds values greater than 2300 for internal cyclone separators indicate the presence of turbulence, which needs to be taken into consideration in the momentum balance. Because of the high velocity and low viscosity of the air

in the pneumatic conveying systems, [29] Reynolds numbers are consistently significantly higher than 2300. The mass and momentum transport equations have the following Reynolds- and time-averaged forms:

$$\frac{\partial \rho}{\partial t} = \nabla \cdot (\rho \overrightarrow{v}) = S_m \tag{30}$$

$$\frac{\partial \rho}{\partial t} + \nabla \rho(\overrightarrow{v} \cdot \overrightarrow{v}) = \nabla \cdot p + \nabla \bar{\bar{T}} + \nabla \rho(\overrightarrow{\overrightarrow{v'} \cdot \overrightarrow{v'}}) + \rho \overrightarrow{g} + \overrightarrow{F} \tag{31}$$

Re-Normalization Group, or RNG, is the model used in the k-ε formulation. It is obtained by applying the renormalization statistical approach to the instantaneous conservation equations. A term added to the ε transport equation improves the prediction of rapidly strained and swirling flows, and an analytical expression for the Prandtl numbers replaces the standard model's previously used constant numbers [29]. These are the main ways in which the RNG model differs from the standard model. The RNG model is generally more trustworthy than the conventional k-ε model due to these enhancements. In order to apply the k-ε method, the transport equations must be solved [30].

$$\frac{\partial \rho k}{\partial t} + \nabla \rho(k \cdot \overrightarrow{v}) = \nabla \cdot \left(\mu + \frac{\mu_T}{\sigma_k} * \nabla k\right) + G_k + G_k + \rho\varepsilon + Y_M + S_k \tag{32}$$

$$\frac{\partial \rho \varepsilon}{\partial t} + \nabla \rho(\varepsilon \cdot \overrightarrow{v}) = \nabla \cdot \left(\mu + \frac{\mu_T}{\sigma_\varepsilon} * \nabla \varepsilon\right) + C_{1\varepsilon}\frac{\varepsilon}{k} + (G_k + C_{3\varepsilon}G_b) - C_{2\varepsilon}\rho\frac{\varepsilon^2}{k} + S_\varepsilon \tag{33}$$

Where Y_M accounts for compressibility effects on turbulence, G_k is the generation of turbulence due to the velocity gradients (local strain), G_b is the generation of turbulence due to buoyancy effects, and σ_k and σ_ε are the turbulent Prandtl numbers for k and ε. $\mathrm{C}_{1\varepsilon}, \mathrm{C}_{2\varepsilon}, \mathrm{C}_{3\varepsilon}$ and in the dissipation rate equation are constants that are derived by calibration with experiments, and Sk and Sε are user defined source terms. The local solution for k-ε enables calculation of the local eddy viscosity, which takes the form:$\mu_T = \rho C_\mu k^2/\varepsilon$. Singh et al. (2023) the eddy viscosity appears in the momentum equations and in the k and ε equations so the solution procedure is strongly coupled.

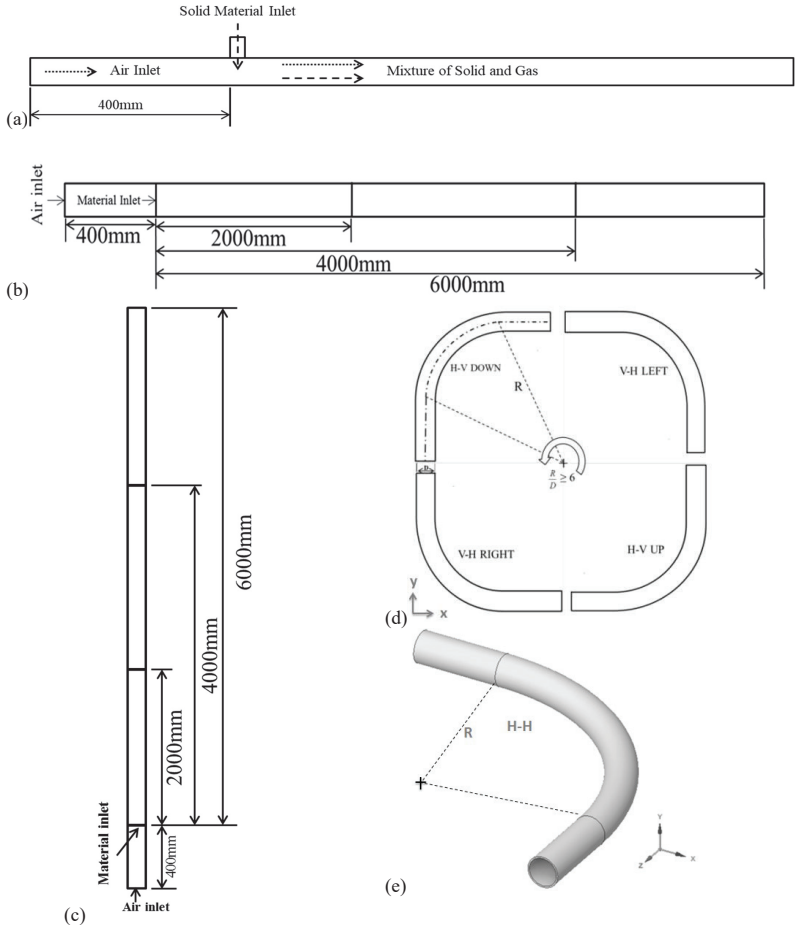

Figure 7 Geometry of (a) feeder, (b) horizontal pipe (c) vertical pipe (d) bends and (e) H-H bend.

3 Results and Discussions

The laboratory and CFD-DPM simulation results presented in this section include the following: pressure drop versus inlet air velocity, pressure drop coefficient versus the square of inlet air velocity, and the ANN model.

3.1 Artificial Neuron Network (ANN) Model

The broad idea of artificial intelligence (AI) is the development of intelligent computers capable of carrying out tasks that traditionally require human

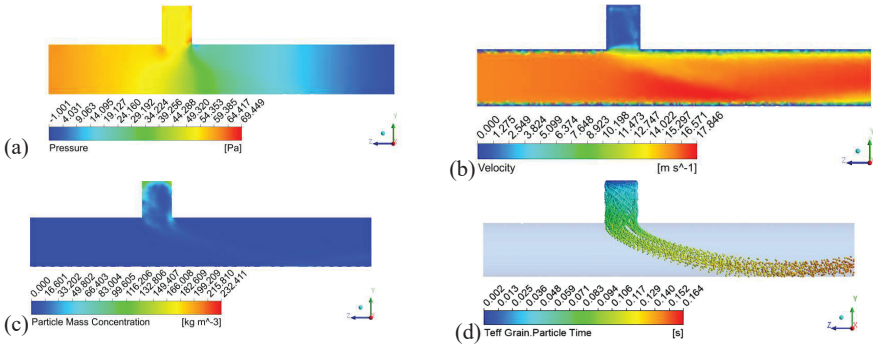

Figure 8 CFD-DPM results for feeder (a) pressure drop (b) air velocity (c) particle mass concentration (d) particle time for D = 46 mm, $m_s = 0.009$kg/s and $v = 16$ m/s.

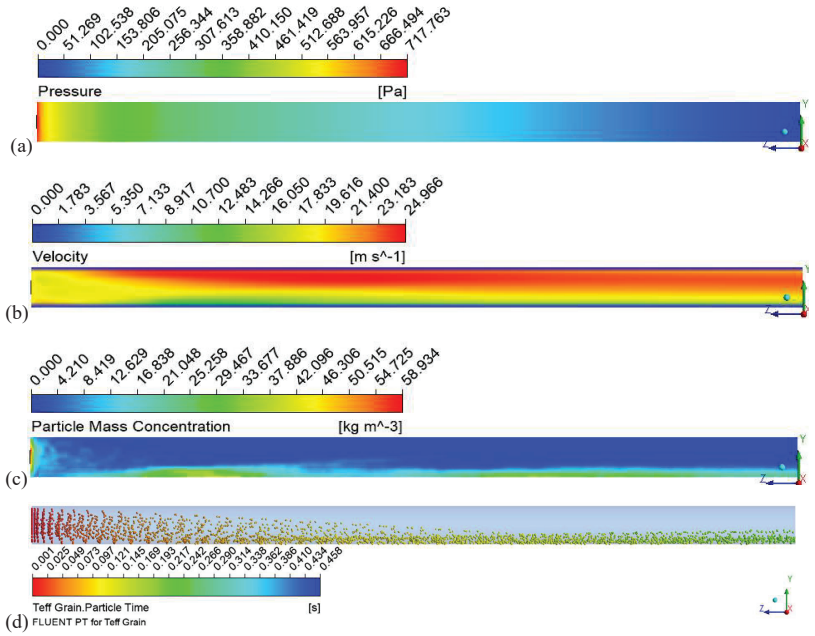

Figure 9 CFD-DPM results for horizontal pipe (a) pressure drop (b) air velocity (c) particle mass concentration (d) particle time for $D = 71$ mm, $L = 4000$ mm, $m_s = 0.13$ kg/s and $v = 20$ m/s.

intelligence. A kind of artificial intelligence called machine learning (ML) enables computers to learn from experience and get better without explicit programming. ML algorithms, as opposed to rule-based programming, use statistical approaches to let machines learn from data to get better at a

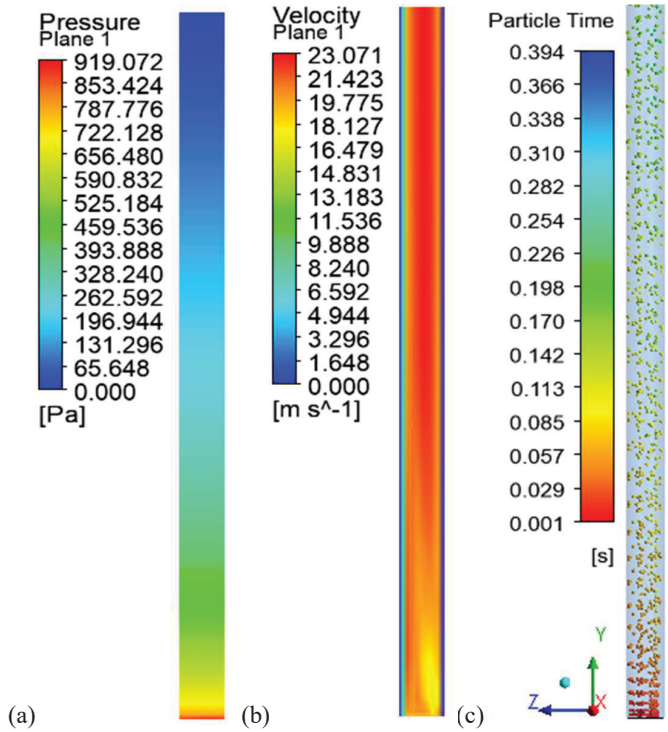

Figure 10 CFD-DPM results for vertical pipe (a) pressure drop (b) air velocity (c) particle time for $D = 71$ mm, $L = 4000$ mm, $m_s = 0.13$ kg/s and $v = 20$ m/s.

particular activity. A branch of machine learning called deep learning (DL) makes use of artificial neural networks which are modeled after the human brain to learn from vast amounts of data. Algorithms that use deep learning have the ability to automatically identify patterns and extract characteristics from data. Deep learning models include artificial neural networks (ANNs) as a crucial component. They are made up of networked nodes with computing and signal transmission capabilities [33].

Pneumatic systems, like many other automated assembly systems, repeat the same sequence. The suggested synthetic data creation approach addressed this issue and made it possible to train and test with ANN. With an average estimation error of less than 1% (with regard to the range) for the training examples, the ANN performed excellently. The average estimation error rose to 2.1% for the test set of data. For the training and test sets, the difference between the perfect and faulty modes was made with absolute assurance.

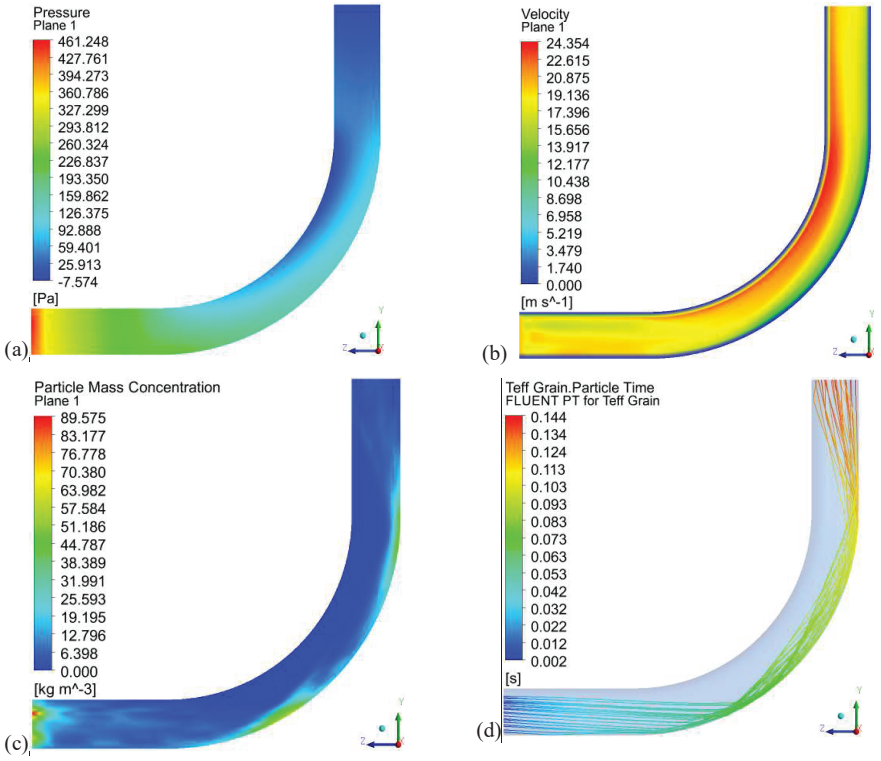

Figure 11 CFD-DPM results for bend (a) pressure drop (b) air velocity (d) particle time for $D = 71$ mm, $L = 4000$mm, $m_s = 0.13$ kg/s and $v = 20$ m/s.

Artificial neural networks (ANNs) have the potential to diagnose even highly repetitive robotic systems [19]. An artificial neural network (ANN) was used to predict the performance of pneumatic conveying of powders. The network was trained using experimental data available for pneumatic conveying, and it was then able to predict the pressure drop using three different training methods: Levenberg Marquardt, Bayesian Regularization, and Scaled Conjugate Gradient [34]. Cyclone pressure drop can be modeled using ANN techniques, which are more accurate than theoretical or semi-empirical models [24]. ANN models can be trained on experimental data of pressure drop measurements across a range of cyclone operating conditions, such as inlet velocity. The ANN model parameters, such as the activation function, need to be carefully selected to optimize the model's performance in predicting pressure drop [35].

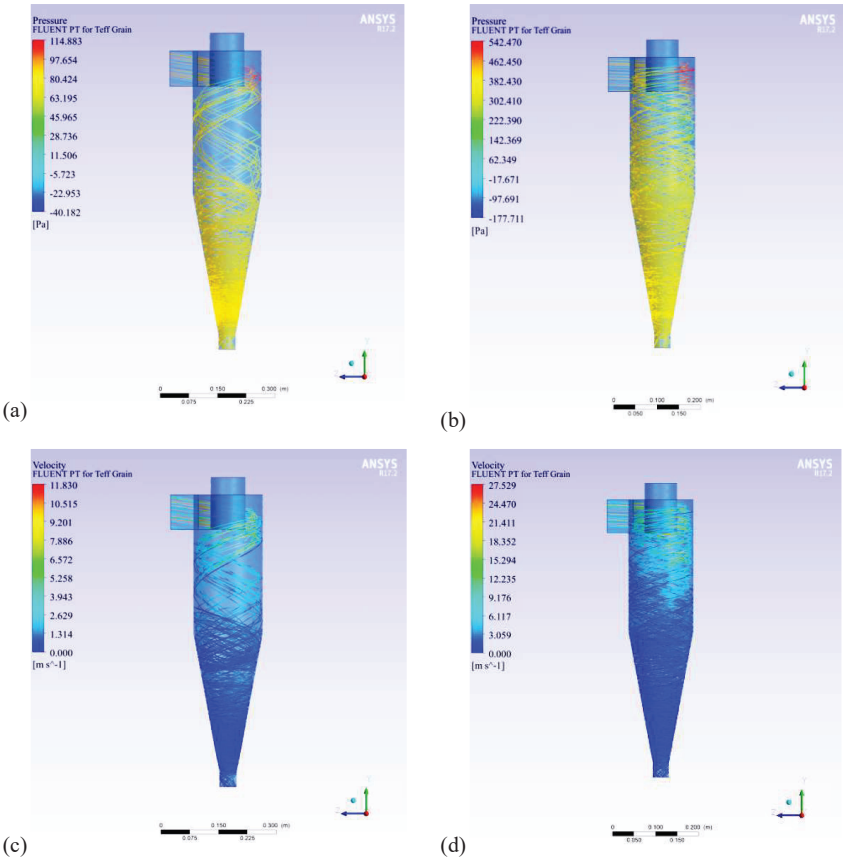

Figure 12 CFD-DPM simulation results for cyclone separator (a) pressure drop at $v = 10$ m/s and $m_s = 0.009$ kg/s (b) pressure drop at $v = 22$ m/s and $m_s = 0.067$ kg/s, (c) air velocity at $v = 10$ m/s and $m_s = 0.009$ kg/s and (d) air velocity at $v = 22$ m/s and $m_s = 0.067$ kg/s for 0.9D cyclone separator.

Three distinct backpropagation techniques were used to train the network: Scaled conjugate gradient, Lavenberg-Marquardt, and Bayesian regularization [36]. The weighted output ($w_{ij}x_i$) is then summed and added to a threshold (θ_j) to produce the neuron input in the output layer.

$$I_j = \sum w_{ij} x_{ij} + \theta_j \tag{34}$$

This input is processed through an activation function f(I_j) at the output layer to produce the output. In this investigation, the tan-sigmoid activation

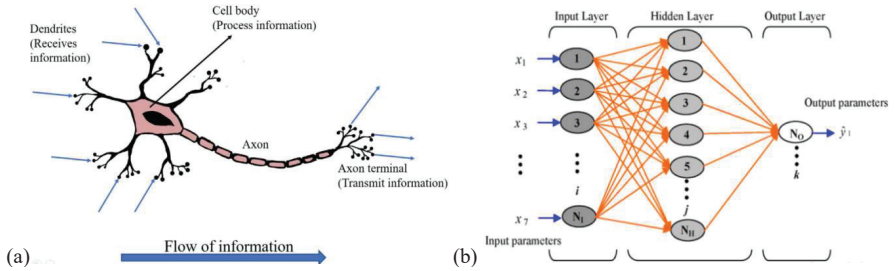

Figure 13 (a) Schematic diagram of feedforward ANN [36], (b) architecture of ANN model [34].

function is employed.

$$Y = f(I_j) = \frac{1}{1 + e^{-2I_j}} - 1 \tag{35}$$

3.1.1 Lavenberg-Marquardt backpropagation algorithm

The purpose of this approach is to achieve second order training speed without computing the Hessian matrix (H). After approximating the Hessian matrix, the gradient (g) is expressed as follows:

$$H = J^T J \tag{36}$$

$$g = J^T e \tag{37}$$

By employing a conventional back propagation technique, one can determine the Jacobian matrix (J) without having to compute the Hessian matrix, hence simplifying the calculation. This approach uses the Newton-like update shown in Eq. to estimate the Hessian matrix.

$$x_{k+1} = x_k - [J^T J + \mu I]^{-1} J^T e \tag{38}$$

When μ is zero, it is just Newton's method, using the approximate Hessian matrix. When μ is large, this becomes gradient descent with a small step size.

3.1.2 Scaled conjugate gradient backpropagation algorithm

$$p_o = -g_o \tag{39}$$

$$x_{k+1} = x_k + \alpha_k g_k \tag{40}$$

$$p_k = -g_k \beta_k p_{k-1} \tag{41}$$

3.1.3 Bayesian regularization backpropagation algorithm

$$F(\omega) = \alpha E_\omega + \beta E_D \tag{42}$$

Where E_ω = Sum of the squared network weights, E_D = Sum of network errors, α and β = factors. Performance of ANN model is evaluated by coefficient of regression (R^2) and mean square error (MSE) were used as the basis of choosing the for best performer train algorithm and expressions of mean square error (MSE), and coefficient of regression (R^2) [34]:

$$MSE = \frac{1}{N}\sum_{i=1}^{N}(\Delta P_{ANN} - \Delta P_{\exp})^2 \tag{43}$$

$$R^2 = 1 - \left[\frac{\sum_{i=1}^{N}(\Delta P_{ANN} - \Delta P_{\exp})^2}{\sum_{i=1}^{N}(\Delta P_{\exp})^2}\right] \tag{44}$$

In testing of ANN model performance, the percentage of the dependent variable's variance that can be predicted from the independent variables is called the Coefficient of Determination (R^2). It has a 0–1 range, with 1 denoting an ideal fit. The mean squared error (MSE) between expected and actual data is calculated lower values are better and 0 means no error.

Figure 16 presented in the figure reveal a robust correlation between the predicted and target values, as evidenced by the high regression coefficients (R^2) calculated for various components of the system. Specifically, the feeder demonstrates an impressive R^2 value of 0.982, indicating an exceptionally close alignment between the predicted outcomes and actual performance. Similarly, the horizontal pipe exhibits an even higher R^2 of 0.989, suggesting that its predictive model is highly reliable. The vertical pipe follows suit with a remarkable R^2 of 0.991, underscoring its effectiveness in accurately predicting performance metrics. Additionally, the bends in the system show a solid correlation with an R^2 value of 0.972, while the cyclone separator, although slightly lower, still maintains a respectable R^2 of 0.942. Collectively, these values not only highlight the accuracy and reliability of the predictive models used for each component but also emphasize their potential utility in optimizing system performance and enhancing operational efficiency across various applications.

Figure 17 highlight that comparison of pressure drop versus inlet air velocity for the feeder, horizontal pipe, vertical pipe, and bends reveals a strong correlation among the experimental data, CFD-DPM results, and the scale-up model. In particular, there is a notable alignment between the

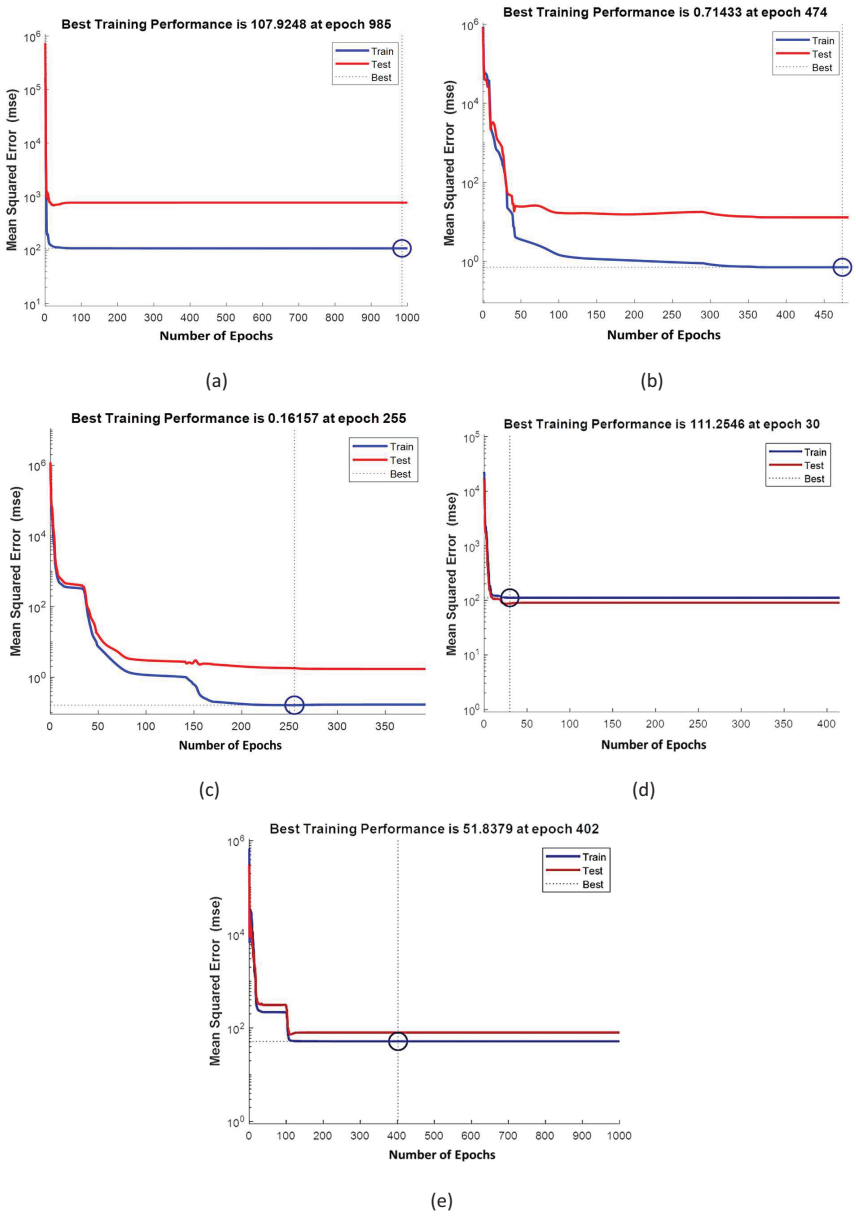

Figure 14 Mean square error (MSE) for (a) feeder, (b) horizontal pipe, (c) vertical pipe, (d) bends, and (e) cyclone separator.

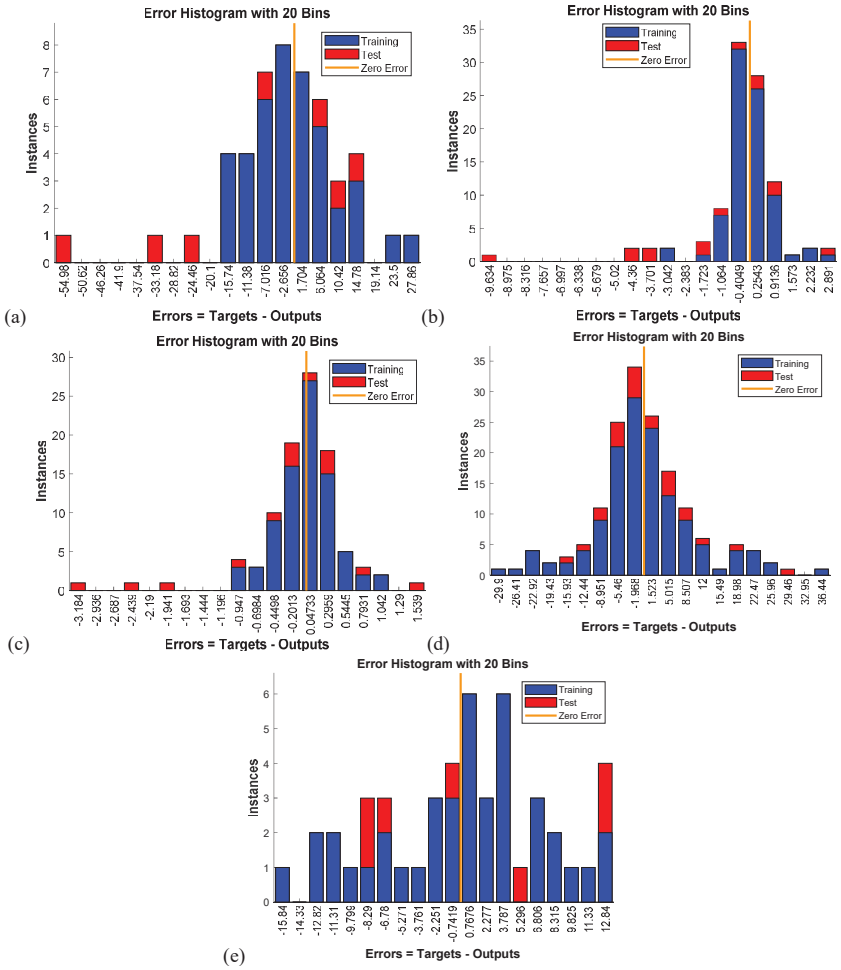

Figure 15 Error histogram for (a) feeder, (b) horizontal pipe, (c) vertical pipe, (d) bends, and (e) cyclone separator.

experimental findings and the CFD-DPM results for the cyclone separator; however, a significant divergence is observed between the Lapple model and the experimental data. The Lapple model, which primarily considers gas characteristics and the number of velocity heads, lacks the depth necessary to accurately account for the complex flow dynamics present in cyclone separators. In contrast, the CFD-DPM approach effectively captures these intricate flow patterns and particle behavior within cyclones under various

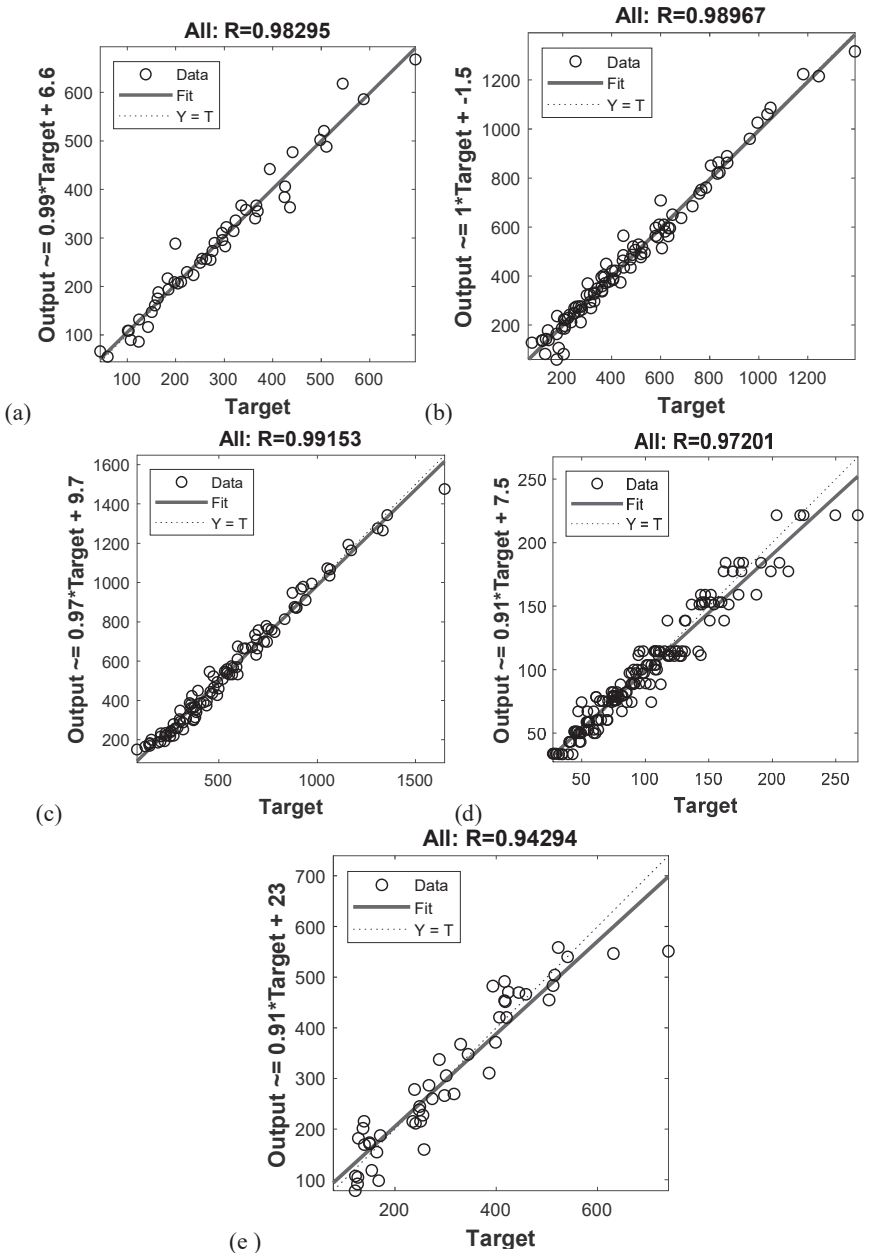

Figure 16 Regression coefficients (R^2) for (a) feeder, (b) horizontal pipe, (c) vertical pipe, (d) bends, and (e) cyclone separator.

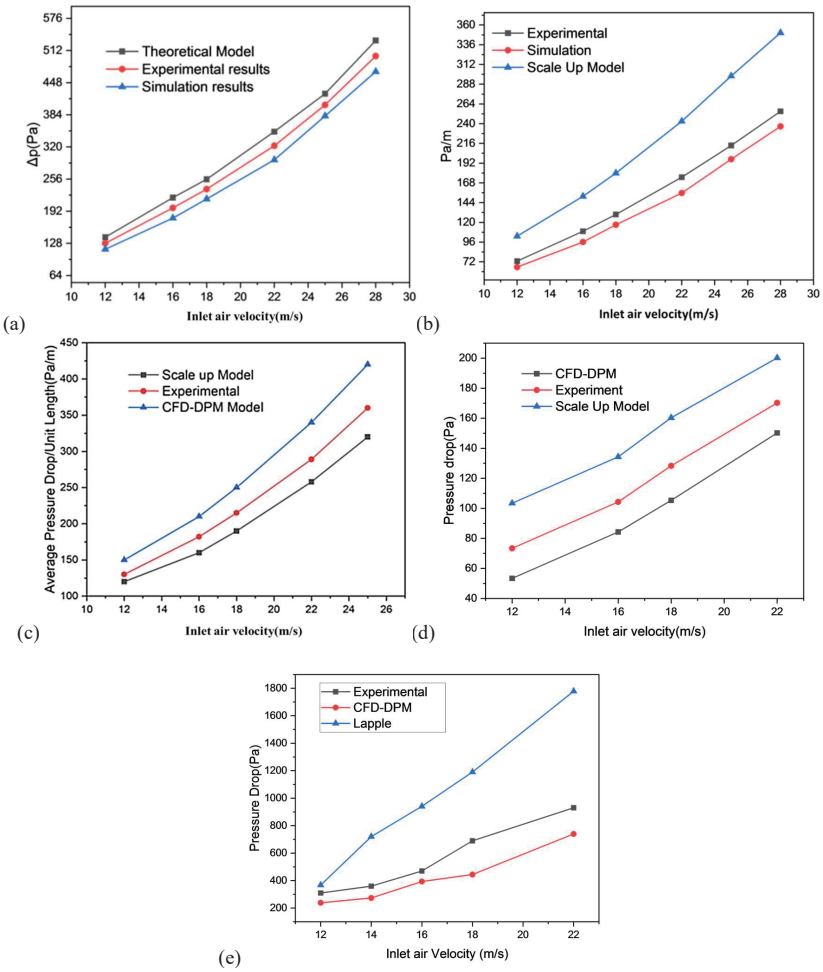

Figure 17 Pressure drop vs. Inlet air velocity for (a) feeder, (b) horizontal pipe, (c) vertical pipe, (d) bends, and (e) cyclone separator.

operating conditions, establishing it as a superior method for predicting pressure drop in cyclone separators.

3.2 Pneumatic Conveyor Scale-up Model

Modeling technique for designing pneumatic conveying systems by addressing the whole pipeline together with all accessories, one method that is used for predicting pressure drop coefficient involves testing a sample of

the product to be conveyed in the final system in a pilot scale rig over a wide range of operating conditions, and measuring the product and air flow rates and resulting pressure drops. The obtained data are then scaled by experimentally determined factors to predict the pressure drop in the full-scale system. The scaling of test data is considered to be one of the most important stages of the design process, in that it provides the link between laboratory-scale apparatus and full-scale industrial installations. Hence, the accuracy and reliability of scale-up are essential. There are two approaches in scaling up techniques available in literature; the Global Approach and the Piecewise Approach. Both approaches have their advantages and undesirable characteristics as well. The basic condition of the technique is that conveying conditions, in terms of air velocities, should be identical for the pilot plant and full-scale plant. It has been revealed that the equations used in Mills scale-up technique are inadequate, especially when data are scaled up concerning pipeline diameter [38]. They proposed following scale-up equation:

$$m_{s2} = m_{s1}\frac{L_1}{L_2}\left(\frac{D_2}{D_1}\right)^{2.8} \tag{45}$$

$$\Delta P = 4\frac{f\rho_a v^2 L}{2D} \tag{46}$$

$$\Delta p_{st} = \frac{1}{2}K_{st}\rho_{sus}v_{entry}^2\frac{\Delta L}{D} \tag{47}$$

In pneumatic conveying systems for pressure drop as a result of bends is calculated using an equation that takes into account frictional losses, solid-to-gas and gas-to-pipe friction, gas and particle acceleration, and the static head of the solids and gas. In order to estimate the pressure reduction in bends, scale up model estimated pressure drop [15]. Equation for pressure drops in bends is:

$$\Delta p_b = \frac{1}{2}K_b\rho_{sus}v_{entry}^2 \tag{48}$$

It should be highlighted that all $\mathrm{v_{entry}}$ value is the true gas velocity at the entry section of the concerned pipe section or pipe component, $K_b =$ pressure drop coefficient for bend pipeline, and suspension density (ρ_{sus}) can be defined as the mixture density when a short pipe element is considered. As an equation, it can be presented in the following way [39].

$$\rho_{sus} = \frac{m_s + m_a}{V_s + V_a} \tag{49}$$

In a pneumatic conveyor, the pressure drop over the feeder is critical to system performance. It controls the flow of both material and air, depending on the air velocity, material properties, and feeder design. It is essential to comprehend this pressure drop in order to maximize transport, avoid obstructions, and improve energy economy and system dependability [40].

$$\Delta P = \frac{1}{2} K \rho_g v_g^2 \tag{50}$$

Where ΔP is pressure drop due to feeder (P_a), ρ_g is the gas density (kg/m^3) and vg is either the inlet or outlet gas velocity (m/s). K is a dimensionless pressure drop coefficient.

A cyclone separator's ability to effectively separate particles from air or gas streams depends on the pressure drop across it. The particle size, flow rate, and separator design are some of the variables that affect this decrease. In many applications, controlling pressure drop is essential to maximizing efficiency and guaranteeing successful separation [9–17].

$$\Delta P_c = \frac{1}{2} \rho_g v_g^2 N_H \tag{51}$$

Where Δ P_c is the cyclone pressure drop (P_a), ρ_g is the gas density (kg/m^3) and v_g is either the inlet or outlet gas velocity (m/s). N_H is a dimensionless pressure drop coefficient and expressed by two parameters.

Figure 18 clearly highlights that the pressure drop coefficient demonstrates the most accurate curve fit when plotted against the square of air velocity for all major components of the system. This trend is particularly evident across various elements, including the feeder, horizontal pipe, vertical pipe, bends, and cyclone separator. Such a strong correlation suggests that as the air velocity increases, the pressure drop experienced by each component follows a predictable pattern based on the square of that velocity. This relationship is crucial for optimizing system performance, as it allows engineers and operators to better understand how changes in air velocity can impact the efficiency and effectiveness of material transport. By identifying these patterns, it becomes possible to fine-tune operational parameters, enhance design considerations, and ultimately improve the overall functionality of the pneumatic conveyor system. The findings underscore the importance of considering these relationships in both theoretical analyses and practical applications within the field.

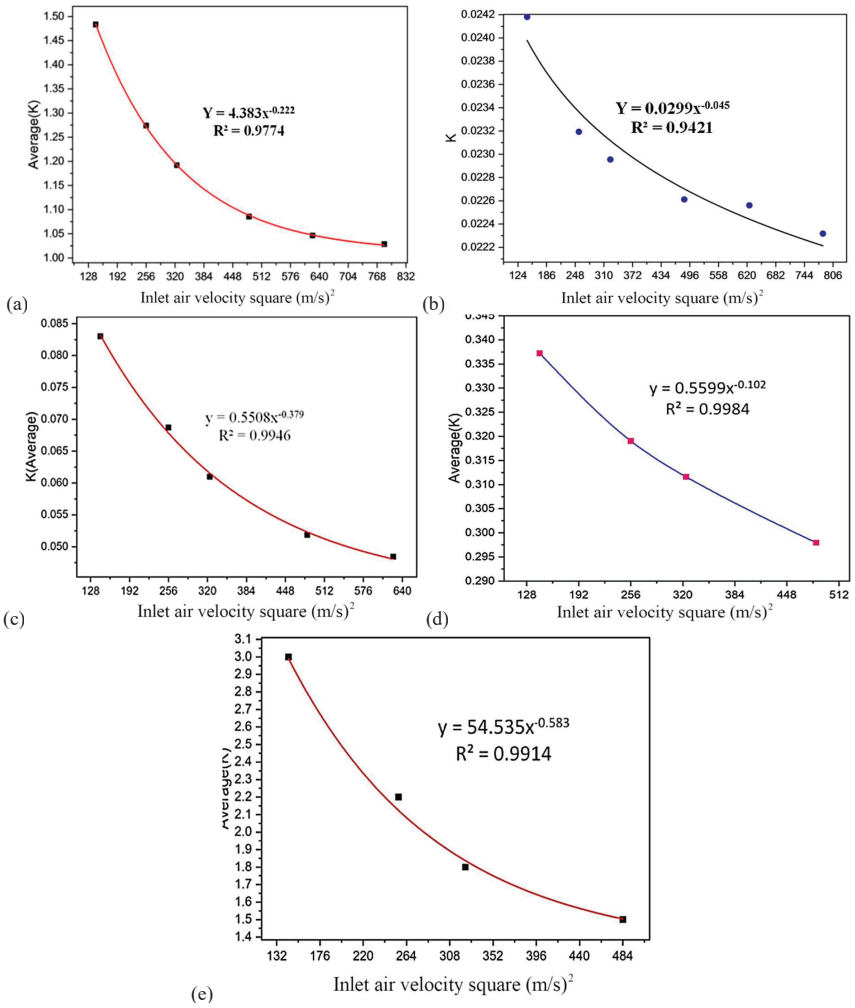

Figure 18 Pressure drop coefficient vs. Inlet air velocity square $(m/s)^2$ for (a) feeder, (b) horizontal pipe, (c) vertical pipe, (d) bends, and (e) cyclone separator.

4 Conclusions

The findings reveal that key components of a positive dilute phase pneumatic teff grain conveyor such as the feeder, horizontal pipe, vertical pipe, bends, and cyclone separator significantly influence pressure drop within the

system. Each component is essential for determining the overall efficiency and performance of the pneumatic Teff grain conveying system.

There are numerous important advantages to combining CFD-DPM simulations and laboratory testing to build artificial neural network models for pressure drop prediction in pneumatic conveying systems. First, important empirical data from laboratory trials can be used to validate CFD simulations, providing a strong foundation for training the ANN models. By ensuring that the simulation results closely match actual circumstances, this empirical data serves to increase the accuracy of the predictions made by the ANN model.

The findings reveal a strong correlation between the calculated pressure drop coefficient (K) and the square of the inlet air velocity, expressed as K α v^2. These results indicate that the model can lead to more efficient designs that accurately reflect real-world conditions, thereby enhancing the overall performance of pneumatic grain conveying systems.

According to the results, Teff grain is moved efficiently by use of a positive dilute phase pneumatic conveyor system, which has been shown to be highly effective in handling this specific grain variety. Having been thought of, this system's efficiency shows how well suited it is to Teff grain's unique properties, which makes it a desirable option for growers and processors looking to improve their operations.

References

[1] G. Abebaw, 2020. The Study of Some Particle Size Distribution of Teff [Eragrostis teff (Zucc.) Trotter] Grain Cultivars and Its Flour, J. Food Nutr. Sci., 8, pp. 108–201.

[2] B. Minten, E. Engida, and S. Tamru, 2016. How big are post-harvest losses in Ethiopia? Evidence from teff, Int. J. Mech. Eng. Appl., 7, p. 89–101.

[3] T. Gonite, 2019. Design and Prototyping of Teff (ጤፍ) Row Planter and Fertilizer Applier, Int. J. Mech. Eng. Appl., 6, p. 91–1015.

[4] T. K. Amentae, E. G. Tura, G. Gebresenbet, and D. Ljungberg, 2016. Exploring value chain and post-harvest losses of Teff in Bacho and Dawo districts of central Ethiopia, J. Stored Prod. Postharvest Res., 7, pp. 11–28.

[5] A. Awgichew, 2019. Aerodynamic Properties of Tef for Separation from Chaff, Civ. Environ. Res., 11, pp. 39–43.

[6] S. Tadić, M. Krstić, M. Božić, S. Dabić-Miletić, and S. Zeèević, 2024. Ranking of Technologies for Intralogistic Bulk Material Handling Processes Using Fuzzy Step-Wise Weight Assessment Ratio Analysis and Axial-Distance-Based Aggregated Measurement Methods, Appl. Sci., 14, pp. 143–167.

[7] L. Stone, D. Hastie, and S. Zigan, 2019. Using a coupled CFD – DPM approach to predict particle settling in a horizontal air stream, Adv. Powder Technol., 30, pp. 869–878.

[8] O. J. I. Kramer et al., 2020. Improvement of voidage prediction in liquid-solid fluidized beds by inclusion of the Froude number in effective drag relations, Int. J. Multiph. Flow, 127, pp. 103–261.

[9] B. Zhao and Y. Su, 2009. Artificial neural network-based modeling of pressure drop coefficient for cyclone separators, Chem. Eng. Res. Des., 88, pp. 606–613.

[10] S. Kuang, M. Zhou, and A. Yu, 2019. CFD-DEM modelling and simulation of pneumatic conveying: A review Powder Technol., 68, pp. 2–23.

[11] S. K. Senapati and S. K. Dash, 2021. Computation of pressure drop for dilute gas–solid suspension across thin and thick orifices, Particuology, 55, pp. 209–221.

[12] S. Kuang, K. Li, and A. Yu, 2020. CFD-DEM Simulation of Large-Scale Dilute-Phase Pneumatic Conveying System, Ind. Eng. Chem. Res., 59, pp. 4150–4160.

[13] S. F. Moujaes and S. Deshmukh, Three-Dimensional CFD Predications and Experimental Comparison of Pressure Drop of Some Common Pipe Fittings in Turbulent Flow, 83, pp. 29–68.

[14] I. Khazaee, 2017. Numerical investigation of the effect of number and shape of inlet of cyclone and particle size on particle separation, Heat Mass Transf. und Stoffuebertragung, 53, pp. 2009–2016.

[15] F. Kaya and I. Karagoz, 2019. Experimental and numerical investigation of pressure drop coefficient and static pressure difference in a tangential inlet cyclone separator, Chem. Pap., 66, pp. 1019–1025.

[16] X. Wu, J. Liu, X. Xu, and Y. Xiao, 2023. Modeling and experimental validation on pressure drop in a reverse-flow cyclone separator at high inlet solid loading, J. Therm. Sci., 20, pp. 343–348.

[17] S. Demir, 2014. A practical model for estimating pressure drop in cyclone separators: An experimental study, Powder Technol., 268, pp. 329–338.

[18] M. E. Orakoglu Firat and O. Atila, 2022. Investigation of the thermal conductivity of soil subjected to freeze–thaw cycles using the artificial neural network model, J. Therm. Anal. Calorim., 147, pp. 8077–8093.
[19] M. Demetgul, I. N. Tansel, and S. Taskin, 2009. Fault diagnosis of pneumatic systems with artificial neural network algorithms, Expert Syst. Appl., 36, pp. 10512–10519.
[20] A. Haghighi, M. S. Shadloo, A. Maleki, and M. Y. Abdollahzadeh Jamalabadi, 2022. Using committee neural network for prediction of pressure drop in two-phase microchannels, Appl. Sci., 10, pp. 15–28.
[21] B. G. Asefa, F. Tsige, M. Mehdi, T. Kore, and A. Lakew, 2023. Rapid classification of tef [Eragrostis tef (Zucc.) Trotter] grain varieties using digital images in combination with multivariate technique, Smart Agric. Technol., vol. 3, pp. 56–83.
[22] B. Zhao, 2009. Modeling pressure drop coefficient for cyclone separators: A support vector machine approach, Chem. Eng. Sci., 64, pp. 4131–4136.
[23] S. Demir, 2014. A practical model for estimating pressure drop in cyclone separators: An experimental study, Powder Technol., 268, pp. 329–338.
[24] B. Zhao and Y. Su, 2009. Chemical Engineering Research and Design Artificial neural network-based modeling of pressure drop coefficient for cyclone separators, Chem. Eng. Res. Des, 88, pp. 606–613.
[25] N. Behera, V. K. Agarwal, M. Jones, and K. C. Williams, 2013. Modeling and analysis of solids friction factor for fluidized dense phase pneumatic conveying of powders, Part. Sci. Technol., 31, pp. 136–146.
[26] K. Sharma, S. S. Mallick, A. Mittal, and P. Wypych, 2023. Modelling solids friction for fluidized dense-phase pneumatic conveying, Part. Sci. Technol., 38, pp. 391–403,.
[27] W. B. Faulkner, B. W. Shaw, an W. B. Faulkner, 2022. Efficiency And Pressure Drop Of Cyclones Across A Range Of Inlet Velocities, Powder Technology, 22, pp. 342–352.
[28] L. Cao, Q. Zhang, and R. Meng, 2022. CFD–DPM Simulation Study of the Effect of Powder Layer Thickness on the SLM Spatter Behavior, Metals (Basel)., 12, pp. 11–28.
[29] F. Huang et al., 2021. Role of CFD based in silico modelling in establishing an in vitro-in vivo correlation of aerosol deposition in the respiratory tract.

[30] C. Wang, W. Li, B. Li, Z. Jia, S. Jiao, and H. Ma, 2023. Study on the Influence of Different Factors on Pneumatic Conveying in Horizontal Pipe, Appl. Sci., 13, pp. 9–23.

[31] P. Dutta, S. K. Saha, N. Nandi, and N. Pal, 2016. Numerical study on flow separation in 90° pipe bend under high Reynolds number by k-ε modelling, Eng. Sci. Technol. an Int. J, 19, pp. 904–910.

[32] J. Singh, H. S. Gill, and H. Vasudev, 2023. Computational fluid dynamics analysis on role of particulate shape and size in erosion of pipe bends, Int. J. Interact. Des. Manuf., 17, pp. 2631–2646.

[33] H. Y. Chiu, H. S. Chao, and Y. M. Chen, 2022. Application of Artificial Intelligence in Lung Cancer. Powder Technology, 511, pp. 204–257.

[34] J. S. Shijo and N. Behera, 2021. Performance prediction of pneumatic conveying of powders using artificial neural network method, Powder Technology, 388, pp. 149–157.

[35] S. Demir, A. Karadeniz, and N. Demir, 2016. Artificial neural network simulation of cyclone pressure drop: Selection of the best activation function in Iraq, Polish J. Environ. Study, 25, pp. 1891–1899.

[36] K. Elsayed and C. Lacor, 2012. Modeling and Pareto optimization of gas cyclone separator performance using RBF type artificial neural networks and genetic algorithms, Powder Technolology, 217, pp. 84–99.

[37] W. Abebe and F. Ronda, 2 015. Flowability, moisture sorption and thermal properties of tef [Eragrostis tef (Zucc.) Trotter] grain flours, J. Cereal Sci. 63, pp. 14–20.

[38] C. Ratnayake, B. K. Datta, and M. C. Melaaen, 2007. A unified scaling-up technique for pneumatic conveying systems, Part. Sci. Technol., 25, pp. 289–302.

[39] B. K. Datta and C. Ratnayaka, 2003. A simple technique for scaling up pneumatic conveying systems, Appl. Sci., 13, pp. 109–230.

[40] E. Fedorova, E. Pupysheva, and V. Morgunov, 2022. Modelling of Red-Mud Particle-Solid Distribution in the Feeder Cup of a Thickener Using the Combined CFD-DPM Approach, Symmetry (Basel)., 14, pp. 141–209.

Biographies

Lemi Demissie Boset, PhD Candidate, is currently pursuing his PhD in Mechanical Engineering at Adama Science and Technology University and serves as a lecturer at Dilla University. He earned his BSc degree in Mechanical Engineering from Wollo University in 2017 and his MSc in Mechanical Design from Addis Ababa University in 2018. His dissertation focuses on Investigation of Teff Grain Characteristics in Positive Dilute Phase Pneumatic Conveyors Using Experimental CFD-DPM Simulation and ANN Modeling Approach. His research interests include agricultural machinery design optimization, Discrete Element Modeling (DEM), Computational Fluid Dynamics (CFD), and machine learning.

Zewdu Abdi Debele, PhD, is currently serving as a faculty member in the Faculty of Agriculture at the University of Eswatini. His academic journey includes positions at Addis Ababa Institute of Technology and Addis Ababa University in Ethiopia, where he was engaged in teaching and research from 2014 to 2016. He earned his PhD from Technische Universität Dresden in

Germany, where he also gained valuable international research experience. His work focuses on the moisture-dependent physical properties of seeds, with notable publications in journals such as Engineering in Agriculture, Environment and Food and Biosystems Engineering.

Amana Wako Koroso, PhD, is a faculty member at Adama Science and Technology University, specializing in Agricultural Machinery Engineering. He earned both his BSc and MSc degrees from Adama Science and Technology University and completed his PhD at Seoul National University, South Korea, in 2016. His doctoral dissertation was titled "Farm Mechanization of Small Farms in Ethiopia: A Case of Cereal Crops in Hetosa District." His research interests include agricultural mechanization and biosystems engineering.